

Magnet design and optimization: The INFN-Genova experience using ANSYS

Stefania Farinon *

Farinon Stefania, INFN - Sezione di Genova, Via Dodecaneso 33, 16146 Genova, Italy

Abstract

ANSYS is a general purpose finite element code that can be used to obtain solutions to a large class of engineering problems involving stress analysis, heat transfer, electromagnetism, fluid flow, as well as many coupled field analyses in one, two or three dimensions. ANSYS is thoroughly effective in tackling all the problems that can be classically dealt with a finite element code. For this reason, the INFN-Genova group adopted ANSYS in 1994, and then followed its evolution and innovation. This paper will highlight the ANSYS most distinguishing features we found out in the last years while designing magnets and electromagnetic devices.

© 2007 Elsevier Ltd. All rights reserved.

Keywords: Magnet design; Finite element analysis

1. Introduction

To date, the finite element method (FEM) is the most widely used numerical method for solving a variety of problems governed by partial differential equations in all areas of engineering. In particular, ANSYS [1] is a complete finite element analysis (FEA) software package which can be used in virtually all fields of engineering. A partial listing of its capabilities contains structural, thermal, low and high-frequency electromagnetics, coupled field, in one, two or three dimensions. The best way to give an idea of its outstanding capabilities is to make a few examples, pointing out some of its special features.

2. Electromagnetic analysis

2.1. Magnetic field accuracy

When designing electromagnetic devices, it is often of basic importance to make very accurate calculations of the magnetic field distribution. To that extent, ANSYS

gives the user the possibility to use the so called “far-field” elements: they allow modeling the effects of far-field decay in magnetic, thermal, and electrostatic analyses without having to specify assumed boundary conditions at the exterior of the model. Consider, for example, the magnetic field produced by the CMS magnet [2], the 4 T, 12.5 m long, 6 m bore diameter superconducting solenoid for the Compact Muon Solenoid experiment at LHC, and its 2-D, axi-symmetric half-symmetry finite element model. Without far-field elements, you would model the air surrounding the iron yoke out to an assumed “infinite” location and then specify either flux-parallel or flux-normal boundary conditions at the edge of the “air” elements, effectively truncating the magnetic effects at that edge. Conversely, introducing the far-field elements the boundary can be relatively close to the model region of interest: the program will take into account the truncation of the magnetic effects at the edges, thus representing the “infinite” boundary of the model. This effect is clearly visible in Fig. 1, representing the flux lines of the magnetic field produced by the CMS solenoid without (a) and with (b) the far-field elements. Without the far-field elements, the flux lines are forced to close artificially at the boundaries, resulting, in this case, in a less accurate evaluation of the fringe field. Indeed, due to the presence of the iron yoke, the difference

* Tel.: +39 010 3536447.

E-mail address: stefania.farinon@ge.infn.it

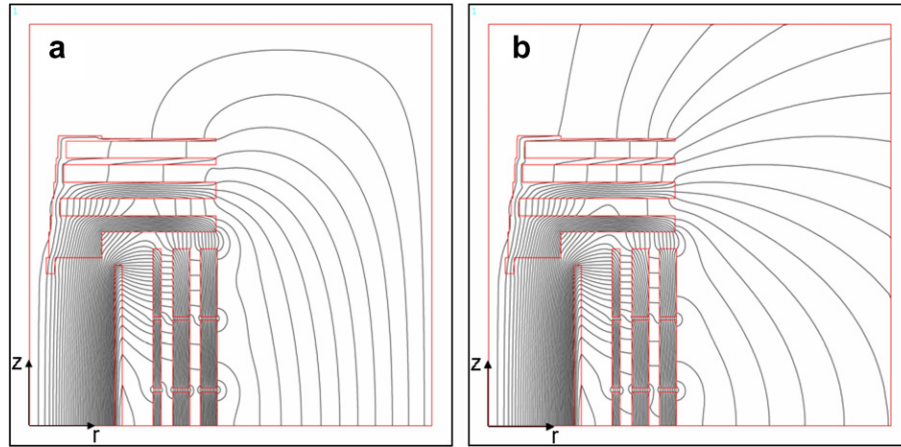


Fig. 1. Flux lines of the magnetic field produced by the CMS magnet without (a) and with (b) far-field elements resulting from a 2D axis-symmetric half-symmetry finite element model.

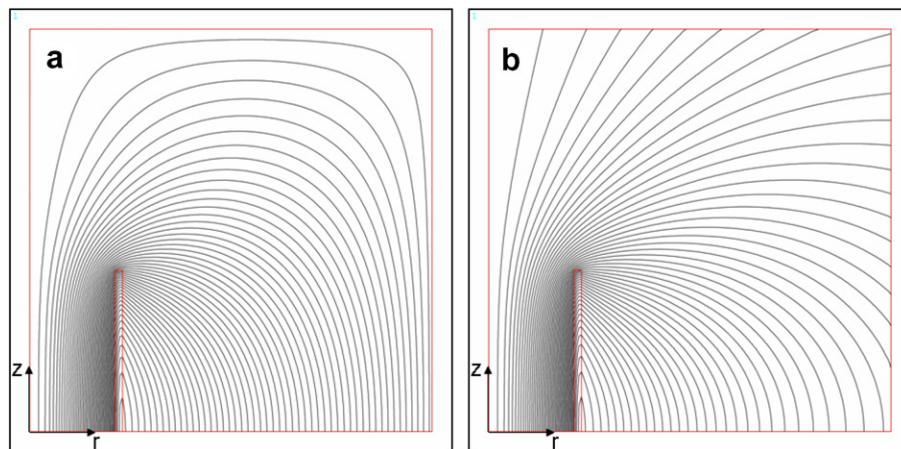


Fig. 2. Flux lines of the magnetic field produced by the CMS solenoid in air without (a) and with (b) far-field elements resulting from a 2D axis-symmetric half-symmetry finite element model.

between the central magnetic field calculated by the two modelizations is about 0.4%. The condition would be much more critical if considering the field produced by the same solenoid in air (see Fig. 2). In this case, comparing the results of the FE analyses with the analytical expression for the central magnetic field obeying Eq. (1) [3], we find that the field calculated without the far-field elements is 1.8% less than its theoretical value, whilst with the far-field elements the field is as accurate as 0.015%.

$$B = \mu_0 J L \ln \left(r_c + \sqrt{r_c^2 + L^2} / r_i + \sqrt{r_i^2 + L^2} \right) \quad (1)$$

Moreover, using the far-field elements, the accuracy in the calculations is not much dependent on the mesh size. For instance, considering again the analysis shown in Fig. 2, using only 800 nodes, we find a central magnetic field as accurate as 0.05%. That accuracy moves to 0.015% by increasing the node number up to only 1300 nodes.

Another powerful tool of the ANSYS program is the possibility to estimate the grade of accuracy of the

electromagnetic finite element analysis, by reproducing the same simulation in several different formulations [4]. Among them, the basic ones are the magnetic scalar potential formulation (MSP), which uses the magnetic scalar potential (MAG) as degree of freedom for the analysis, and the magnetic vector potential formulation (MVP) which uses the three components of the magnetic vector potential (A_X , A_Y and A_Z) as degrees of freedom for the analysis. It can be demonstrated that the MSP formulation converges to the exact energy from above, whilst the MVP formulation converges to the exact energy from below. This means that, when accuracy is a critical factor, the best way to tackle an electromagnetic analysis is to run both the formulations: the difference between the two is the best measure of the accuracy.

As an example, let us consider again the magnetic field produced by the CMS solenoid in air. Fig. 3 shows the magnetic field along the axis of the CMS magnet near the mid-plane for MSP formulation, MVP formulation and analytical expression. If we compare the finite element

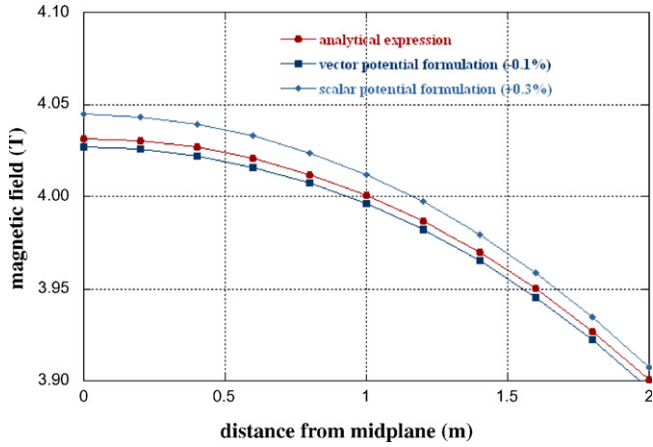


Fig. 3. Magnetic field along the axis of the CMS magnet near the mid-plane: comparison among MSP formulation, MVP formulation and analytical expression.

analyses with the analytical expression for the field along the magnet axis, which can be easily found by extending Eq. (1), it is possible to verify what previously stated: the vector potential formulation is an approximation by defect

of the magnetic field, whilst the scalar potential formulation is an approximation by excess of the magnetic field.

2.2. Optimization using a genetic algorithm

Another interesting feature of ANSYS program, showing its high grade of flexibility, is the possibility to use it as a mere subroutine of any other external program. Parameters can be either directly passed or exchanged through external files. As the ANSYS internal optimization techniques are not particularly efficient, a typical example is the implementation of the ANSYS program in an external optimization algorithm. In particular, we implemented ANSYS in an existing genetic algorithm, written in Fortran, where ANSYS is only a mathematical operator able to calculate the objective function [5]. As an example, let us consider the 4.5 T 92 mm diameter bore dipole shown in Fig. 4, made by 32 turns distributed in four blocks. We used the genetic algorithm to optimize the first five non-zero harmonic components of the magnetic field calculated at a reference radius of 30 mm. The parameters taken into consideration for the optimization are nine, both continuous and discrete, describing the angular position of the

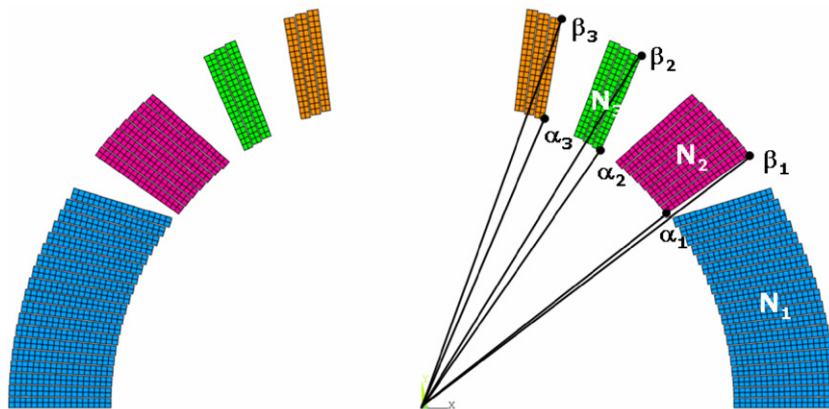


Fig. 4. Schematic section of 4.5 T 92 mm bore dipole, showing the optimization parameters used in the genetic algorithm.

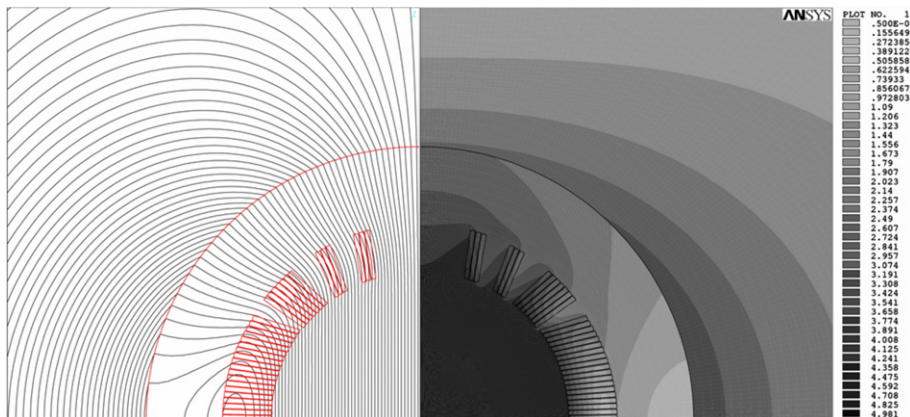


Fig. 5. Magnetic field (on the right) and flux lines (on the left) of the optimized 4.5 T 92 mm bore dipole.

blocks (six parameters) and number of turns in each block (three parameters). Dealing with a genetic algorithm, we can choose as objective function a non-continuous and non-derivable function representing the maximum in absolute value among the first five odd harmonics ($\max[|b_3|, |b_5|, |b_7|, |b_9|, |b_{11}|]$). In less than 200 generations we found a solution where all the harmonics are below one unit: $b_3 = 0.7$ units, $b_5 = 0.8$ units, $b_7 = 0.8$ units, $b_9 = 0.3$ units and $b_{11} = 0.3$ units. Fig. 5 shows the magnetic field and the flux lines of the optimized configuration.

3. Structural analysis

3.1. Large deformation of plastic materials

The analyses involving large deformation of plastic materials are usually very complicated to be tackled and often generate problems of convergence to the finite element codes. In this frame, ANSYS developed a particularly efficient generation of elements for modeling solid structures, which can effectively handle analyses involving plasticity, large deflection, large strain, even in presence of contact. In particular, the contact elements overlay in its boundary the solid elements describing a deformable body. There is a wide set of features which can be tuned to give a proper description of the contact surfaces and their pairing. For instance, the contact can be either rigid-to-flexible or flexible-to-flexible, there can be sliding with or without friction, it is possible to impose an initial adjustment able to close gaps or reduce penetration.

As an example, consider the Nb₃Sn Powder in Tube wire developed by SMI for the NED experiment [6] and shown in Fig. 6 together with the finite element model used for the analysis [7]. In the model, all the mechanical material properties are represented by bi-linear stress–strain curves: this option uses the von Mises yield criteria coupled with an

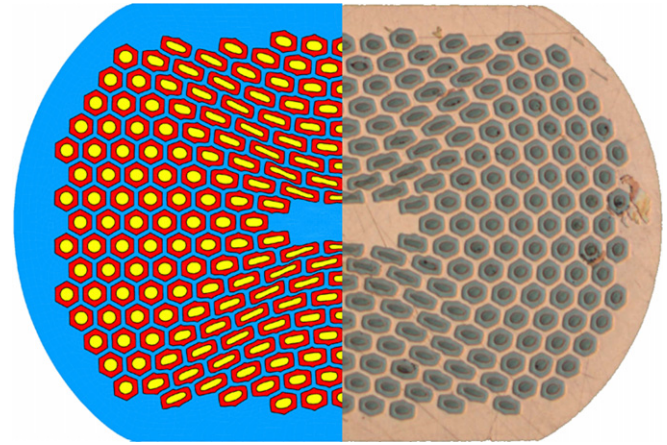


Fig. 7. SMI/NED PIT wire after a 24% reduction in diameter. The observed deformation is shown together with the FE analysis result.

isotropic work hardening assumption and it is preferred for large strain analyses. In our case, the main advantage consists in the fact that it needs only three parameters, the Young modulus, the yield strength and the second slope. Therefore, it enables keeping the FE model behavior under control and isolating the basic influence of each parameter on the final results.

Let us suppose to compress the wire between two rigid and parallel walls using the ANSYS contact technology (contact elements have been modeled between the walls and the external surface of the wire). In Fig. 7 there is a comparison between the observed deformation and the calculation corresponding to a total reduction in diameter of 24%. The match is not perfect, but the calculations give a suitable description of the overall behavior of the real wire. Two shear planes tilted by about 45° with respect to the x -axis can be easily identified. They divide up the x - y plane into four regions: the regions on both sides are almost

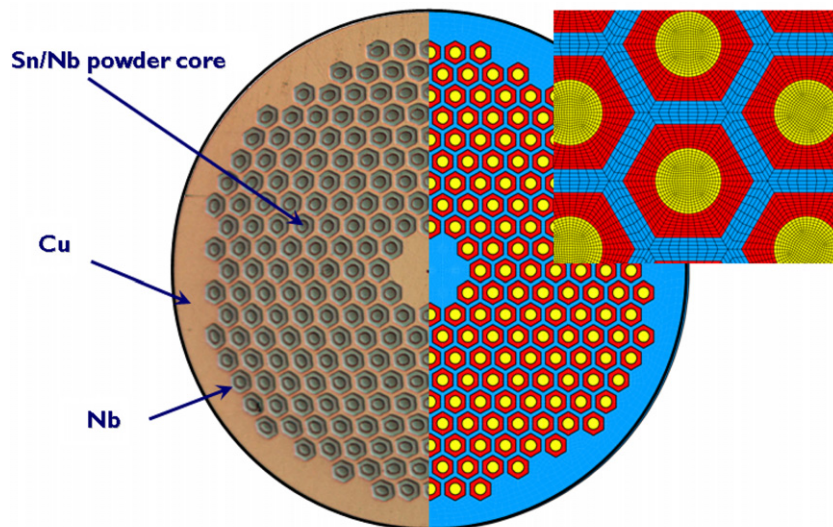


Fig. 6. SMI/NED PIT wire shown together with its FE model (about 100,000 nodes). White represents Sn/Nb powder core, light grey is copper and dark grey is niobium. The wire diameter is 1.25 mm.

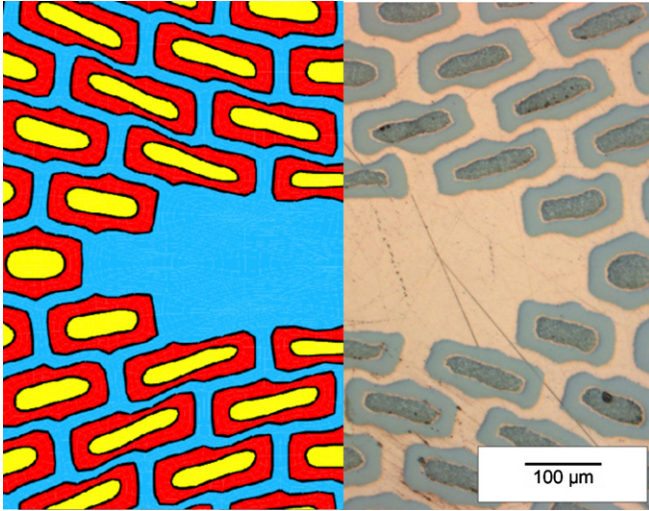


Fig. 8. SMI/NED PIT wire after a 24% reduction in diameter enlarged in the around the center of the wire. The observed deformation is shown together with the FE analysis result.

unaffected by the deformation, whilst the top and bottom regions are the most strained, especially near the center of the wire. In Fig. 8 an enlargement of the previous picture around the center of the wire is shown. It is possible to appreciate that there is a sort of “bumping” effect on the central tubes which is well predicted by the FE analysis.

In this work, we intended to demonstrate that FE analysis is a powerful tool to simulate severe plastic deformations of wires. It can be adopted to predict the mechanical behavior during cabling of different strand designs, with the aim to find an optimum design minimizing cabling damages.

4. Multiphysic simulations

4.1. Coupled thermal electric transient analysis

An example of a rather complicated coupled thermal electric transient analysis is the simulation of the thermal behavior of a superconducting magnet during a quench [8]. The only input needed for this kind of analysis, besides the appropriate material properties, is the rule of the current decay after a quench is detected. If we consider a basic protection circuit, an external resistance R_e in parallel to the superconducting magnet, when a quench is detected the current starts to decay with a simple exponential law:

$$I(T, t) = I_0 e^{-\frac{R_e + r_i(T,t)}{L} t} \quad (2)$$

where L and $r_i(T, t)$ are, respectively, the inductance and the internal resistance as function of temperature and time of the superconducting magnet. Next step is to define a logical algorithm for this analysis. Let us start from an initial situation with null internal resistance, where the circulating current is the operating one, the temperature is the operative one everywhere but the region where the quench starts,

and the temperature is arbitrarily set to a higher value. Due to the local raise of temperature, it happens that the internal resistance $r_i(T, t)$ grows. Following Eq. (2), we have a corresponding decay of the current circulating in the magnet and, consequently, a new value of resistivity $\rho(T, t)$ for the material defining the conductor. Choosing for instance a copper based conductor, and including the current sharing effect, that resistivity can be represented by Eq. (3):

$$\rho(T, t) = \begin{cases} \rho_{SC} & T < T_g(T, t) \\ \rho_{SC} + \rho_{Cu}(T) \frac{T - T_g(T, t)}{T_C - T_g(T, t)} & T_g(T, t) < T < T_C \\ \rho_{Cu}(T) & T > T_C \end{cases} \quad (3)$$

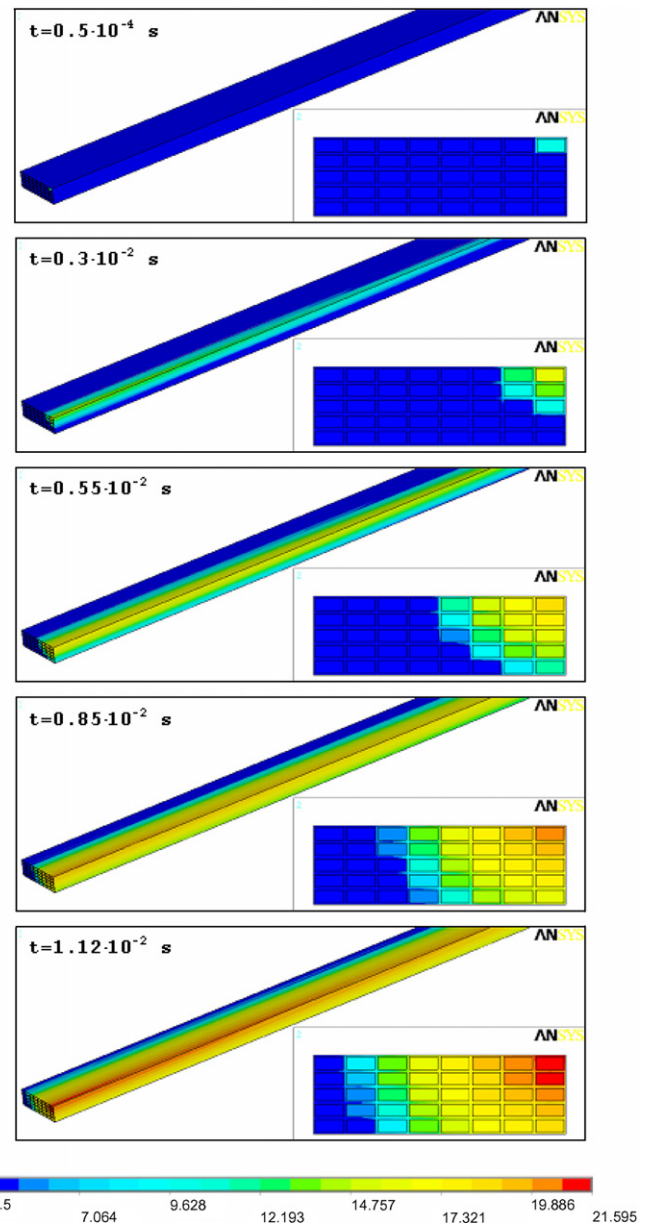


Fig. 9. Example of a thermal electric transient analysis: temperature profile as function of time in a rectangular winding. At $t = 0^+$, the temperature of the right top conductor has been raised to 10 K. The system is supposed to be adiabatic.

where ρ_{SC} is the resistivity of superconductor (nearly zero), $\rho_{Cu}(T)$ is the resistivity as function of temperature of copper, T_C is the critical temperature of superconductor, and $T_g(T, t)$ is the sharing temperature, defined as: $T_g(T, t) = T_C - (T_C - T_0)I(T, t)/I_C$. The consequence is that when the current starts to decay, also the resistivity of conductor, through their sharing temperature, changes.

In other words, the idea at the basis of this analysis is that the values of resistance at time t , simply obtained as the ratio between the dissipated power and the square of the current circulating at the time t , allows calculating the loading conditions at the time $t + \Delta t$, that is the new values of the decayed operating current and resistivity.

An example of how this procedure works is show in Fig. 9, corresponding to the thermal transient of a rectangular winding made of 40 insulated turns. At time $t = 0^+$, the temperature of one face of the top right conductor is raised up to 10 K. No cooling is present, that is the temperature diffusion is supposed to be adiabatic. Fig. 9 represents the evolution in time of the temperature profile in the winding.

What it is very interesting are the potentials of this analysis. First of all, it is possible to take into account any kind of boundary conditions, the presence of possible cooling, or potential source of thermal disturbances, by simply adding the desired loads to the finite element model. Second, it is possible to solve the problem in case of a different protection circuit or not detected quench, by simply changing the law of current decay. And finally, as time by time ANSYS computes the temperature distributions, these distributions

can be used as input loads of structural analyses, in such a way to calculate the stress maps as function of time during the quench propagation.

5. Conclusion

I think that the ANSYS program has widely demonstrated to be a powerful tool in magnet design. Its main advantage consists in the fact that it continuously evolves following the progress of calculation tools and the need of users.

References

- [1] ANSYS® Inc., revision 10.0 (www.ansys.com).
- [2] Kircher F et al. Final design of the CMS solenoid cold mass. IEEE Trans Appl Supercond 2000;10(1).
- [3] Wilson MN. Superconducting magnets. Oxford Science Publication.
- [4] Preis K, Bardi I, Biro O, Magele C, Vrisk G, Richter KR. Different finite element formulations of 3D magnetostatic fields. IEEE Trans Magnet 1992;28(2).
- [5] Priano C, Fabbriatore P, Farinon S, Musenich R, Perrella M, Squarcia S. A superconducting magnet for a beam delivery system for carbon ion cancer therapy. IEEE Trans Appl Supercond 2002;12(1).
- [6] Devred A et al. Overview and status of the Next European Dipole joint research activity. Supercond Sci Technol 2006;19:S67–83.
- [7] Farinon S, Boutboul T, Devred A, Fabbriatore P, Leroy D, Oberli L. FE model to study the deformations of Nb3Sn wires for the Next European Dipole (NED). IEEE Trans Appl Supercond 2007;17(2).
- [8] Caspi S et al. Calculating quench propagation with ANSYS. IEEE Trans Appl Supercond 2003;13(2).